Journal of Global Positioning Systems (2025)
Vol. 21, Issue 1: 30-43
DOI:10.5081/jgps.21.1.30

Analysis of GPS Network Inversion Filtering Algorithms for Fault Slip

Zhengdong Luo[2], Tieding Lu[1,2,3,4]✉, Qianru Chen[2], Xiwen Sun[2], Weijian Hu[2]

1 National Key Laboratory of Uranium Resource Exploration-Mining and Nuclear Remote Sensing, Nanchang, 330013, China
2 School of Surveying and Geoinformation Engineering , East China University of Technology, Nanchang, 330013, China
3 Key Laboratory of Mine Environmental Monitoring and Improving around Poyang Lake of Ministry of Natural Resources, East China University of Technology, Nanchang, 330013, China
4 Jiangxi Key Laboratory of Watershed Ecological Process and Information (Platform No. 2023SSY01051), East China University of Technology, Nanchang, 330013, China
✉ Correspondence, tdlu@whu.edu.cn

Abstract: Our study employs GPS coordinate time series and the NIF method to invert postseismic deformation, investigate the spatiotemporal evolution of fault slip, and evaluate the inversion efficiency of the NIF method under various parameter settings, thereby providing prior information for future research on earthquakes and fault slip. Taking the GPS coordinate time series from the Tokai region of Japan during 2009-2021 as an example, we conducted an analysis using the NIF method. The results indicate that the fault slip following the 2011 earthquake was primarily concentrated in the northeastern part of Tokai region (34.8°N-35.8°N, 137.2°E-138.4°E), with a maximum cumulative slip of 9.31 cm at depths ranging from 20 to 60 km. In terms of model parameter analysis, the inversion time and memory cost increase with the number of sub-faults, while the maximum cumulative slip approaches a stable value. Variations in the proportion of local benchmark motion proportion parameter do not affect the inversion time or memory cost but are negatively correlated with the maximum cumulative slip. The time scale of the GPS coordinate time series has no significant impact on the NIF inversion. In contrast, higher time resolution of the GPS coordinate time series results in longer inversion times and greater memory cost, with the maximum cumulative slip gradually stabilizing.

Keywords: Global positioning system coordinate time series; Network inversion filter (NIF); postseismic deformation; Spatiotemporal evolution characteristics

1. Introduction

Earthquakes are natural disasters caused by the mutual compression and collision between tectonic plates, leading to faulting or fracturing along and within the plate boundaries. During an earthquake, only a portion of the elastic strain energy accumulated during the seismic process is released by the Earth's crust. The majority of the energy is instead released through aseismic slip, such as postseismic afterslip and slow slip[1, 2]. Concurrently, with the advancement of Global Positioning System (GPS) monitoring technology, GPS enables the precise measurement of millimeter scale surface deformation caused by postseismic slip[3], thereby providing high-precision and high-temporal-resolution data for the inversion of postseismic slip events. Therefore, utilizing GPS coordinate time series in conjunction with slip inversion methods to reconstruct the spatiotemporal distribution and evolution of postseismic slip can enhance our understanding of fault slip mechanisms and kinematics. This approach is of significant importance for seismic hazard assessment and the study of earthquake generation processes.

Numerous studies have employed various slip inversion methods to obtain the spatiotemporal distribution and evolution of fault slip in different regions. Sun et al. utilized the Sensitivity based Iterative Fitting method to invert the postseismic deformation mechanism of the 2008 Yutian, Xinjiang, Ms 7.3 earthquake[4]. The results indicated that the maximum cumulative surface deformation reached 15 cm after 782 days, and postseismic fault afterslip is likely the dominant mechanism for the observed deformation[5]. Hong et al. employed the Steepest Descent Method (SDM) to invert the postseismic afterslip of the 2008 Damxung, Tibet, Mw 6.3 earthquake[6]. The inversion results indicated that the afterslip primarily occurred at depths of 0-15 km, with a maximum cumulative slip of approximately 0.07 m. After 665 days, the afterslip released a seismic moment of 1.92×10^{17} N·m, accounting for approximately 4.8% of the seismic moment energy released during the coseismic slip[7]. Li et al. constructed a dual slope geometry model based on triangular dislocation elements to invert the postseismic afterslip of the 2015 Mw 7.9 Nepal earthquake[8]. The results showed that the depth distribution of the afterslip was generally greater than 25 km, with a maximum cumulative afterslip of 0.5 m. The released seismic moment energy was 1.02×10^{20} N·m, accounting for approximately 12% of the seismic moment released during the mainshock. Yang et al. based on the theory of elastic dislocation, employed the Principal Component Analysis based Inversion Method (PCAIM) to analyze the spatiotemporal characteristics of postseismic fault slip following the 2015 Mw 7.9 Nepal earthquake[9]. The results indicated that the afterslip was primarily located at a depth of 26.7 km, with a maximum slip of 20.6 cm and a released seismic moment of approximately 3.36×10^{20} N·m. Li et al. utilized GPS coordinate time series and the Principal Component Analysis based Inversion Method (PCAIM) to detect three slow slip events (SSEs) off the Boso Peninsula, Japan, from 2011 to 2019[10]. By analyzing the spatiotemporal evolution of the slip, they revealed different nucleation mechanisms for these events and inferred that the recurrence interval of SSEs in the region is approximately 4-7 years. Yamagiwa et al. conducted a joint inversion of postseismic deformation following the 2011 great east Japan earthquake (Mw 9.0) using combined GEONET and seafloor GPS/Acoustic observation data[11]. Their results indicated that the postseismic deformation was not solely due to shallow afterslip: the afterslip was mainly distributed along the downward extension of the aftershock rupture zone, while the longer-term sustained deformation was closely related to viscoelastic relaxation in the lower crust and upper mantle. Their study emphasized the importance of joint constraints from terrestrial and seafloor observations and pointed out that deep rheological processes play a critical role in maintaining postseismic deformation over multiple years, providing a valid physical basis for explaining the post-seismic signals in central Japan. Liu et al. utilized GNSS coordinate time series from 215 stations across the Japanese islands, combined with spherical dislocation theory, to invert for the afterslip distribution and evolution process of the great east Japan earthquake[12]. Their findings showed that fault afterslip primarily occurred in the initial post-seismic period (within six months), decayed rapidly over time, and essentially ceased around two years after the earthquake. The mantle viscoelastic relaxation effect progressively dominated over time, exceeding the fault afterslip effect approximately four years postseismic. These insights offer a reliable physical explanation for understanding the postseismic evolution of the Japan trench. Segall et al. were the first to propose the concept of GPS network inversion filtering for inversion and subsequently developed the Network Inversion Filter (NIF) to invert for postseismic afterslip and slow slip events[13]. NIF is an effective method for inverting time-dependent fault slip based on GPS coordinate time series. It employs temporal smoothing regularization of fault slip without assuming any specific functional form, allowing slip evolution to be recovered at arbitrary times as long as the slip varies smoothly to a certain extent. Compared to fault slip inversion methods that rely on a limited number of temporal basis or smoothing functions, NIF offers

significantly higher temporal resolution in slip estimates[14-16].

This study will utilize GPS coordinate time series and the NIF method to invert postseismic deformation. Taking the postseismic deformation event in Tokai region following the 2011 Mw 9.0 Japan earthquake as an example, we employ GPS coordinate time series from 2011 to 2021 in the region combined with the NIF method. We analyze the impacts of different model parameters and GPS coordinate time series with varying time scales and temporal resolutions on the inversion time, data memory cost, and fault slip amount. This approach allows us to investigate the spatiotemporal evolution characteristics of the fault slip in the region.

2. Data and methodology

2.1 Regional tectonic setting and observational data

The Tokai region in central Japan is located at the junction of the Amur Plate, Philippine Plate, and Okhotsk Plate. The Philippine Plate is subducting beneath the Amur Plate at a rate of approximately 5.5 cm/year in a northwestward direction, as shown in Figure 1(a)[17]. The data used in this study are daily GPS coordinate time series from 2011 to 2021, obtained from the GEONET (GPS Earth Observation Network System) continuous observation network in the Tokai region of Japan. The solutions were processed by the Nevada Geodetic Laboratory using the GIPSY/OASIS software, based on the IGS08 reference frame. Detailed processing strategies can be found at: http://geodesy.unr.edu/. The precision of the GPS single-day solution coordinate time series is within 2 mm in the horizontal (east and north) directions and within 3 mm in the vertical (up) direction. The distribution of the 124 GPS stations in the Tokai region of Japan is shown in Figure 1(b).

On March 11, 2011, the Mw 9.0 great east Japan earthquake occurred off the Tohoku region of Japan (location shown by the yellow pentagram in Figure 1(a)), representing one of the strongest subduction zone megathrust earthquakes in global history. The earthquake took place along the Japan trench, where the Pacific Plate subducts westward beneath the North American Plate, triggering significant plate interface rupture and massive seafloor displacement. The rupture extended over 450 km, with a maximum co-seismic slip of nearly 50 m. This event induced widespread crustal deformation in Japan and surrounding areas, followed by a multi-year post-seismic evolution process involving shallow afterslip and deep viscoelastic relaxation. Consequently, the Mw 9.0 great east Japan earthquake has become a crucial case study for investigating plate boundary mechanics, postseismic deformation mechanisms, and the seismic cycle evolution[18,19].

2.2 Network Inversion Filtering Algorithms

GPS network inversion and filtering mainly use the surface displacement signals $u(x,t)$ monitored by the GPS observation network to invert fault slip amounts[13]. The functional model is shown as follows:

$$u_r(x,t) = \int_A G^r_{pq}(x,\xi) s_p(\xi,t) dA(\xi) + L(x,t) + f(t) + e(x,t) \quad (1)$$

where $u_r(x,t)$ represents the surface displacement signals monitored by GPS, x denotes the GPS station coordinates, and t indicates the observation time. r, p, and q represent the north (N), east (E), and up (U) components of the observed displacement, estimated displacement, and fault slip. $G^r_{pq}(x,t)s_p(\xi,t)dA(\xi)$ represents the surface displacement resulting from cumulative slip $s_p(\xi,t)$ at point ξ on fault plane $A(\xi)$ in a homogeneous elastic half-space. $G^r_{pq}(x,\xi)$ denotes the elastic Green's function that relates the cumulative slip at point ξ on the fault plane to the surface displacement at point x. $L(x,t)$ represents the local reference motion that is time-dependent, $f(t)$ denotes the common mode error that is space-related, and $e(x,t)$ is the random noise.

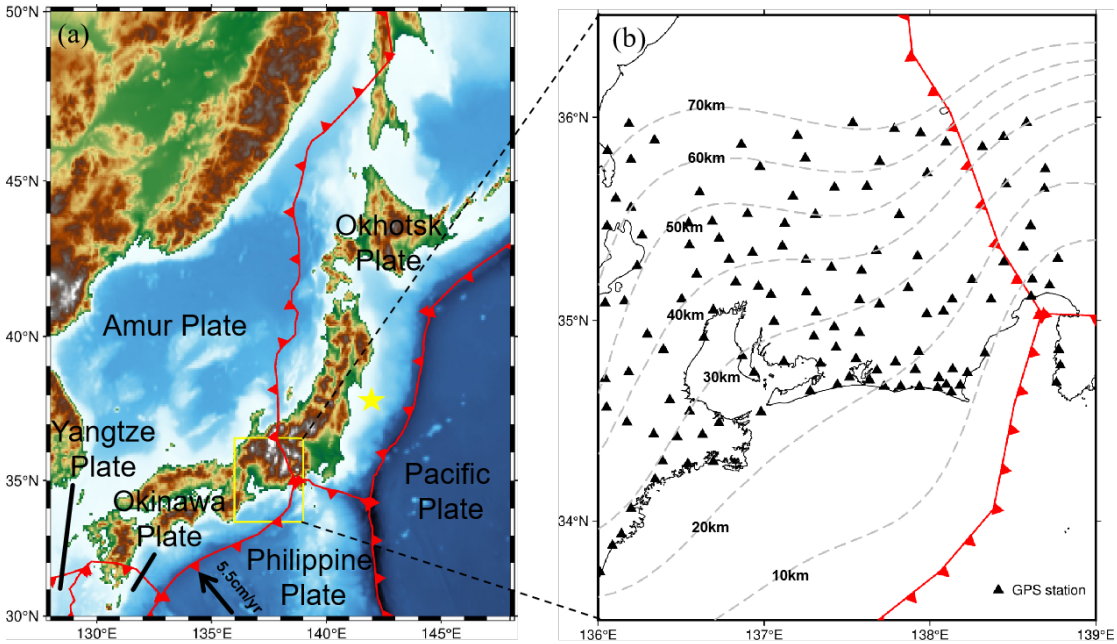

Figure 1. Tectonic Background and Spatial Distribution of Continuous GPS Stations in Tokai region of Japan

In this method, the surface displacement signals monitored by GPS are known quantities. The fault plane and Green's functions can be generated based on regional geological structural data and the dislocation model in an elastic homogeneous half-space and are thus considered known quantities. The unknowns mainly include the fault slip, random reference motion, and common mode error. If the GPS observation network consists of N stations, the displacement components amount to 3N. Therefore, the observation vector d can be expressed as:

$$d_i(t) = u_r(x_n, t) \quad (n = 1, 2, \ldots, N; i = 3(n-1) + r) \quad (2)$$

After constructing the fault plane, it is typically divided into several subfault patches based on the fault's size. Let M be the number of subfaults, corresponding to M spatial basis functions. The fault slip can then be expressed as a linear combination of the spatial basis functions $B(\xi)$:

$$s_p(\xi, t) = \sum_{k=1}^{M} c_k^{(p)}(t) B_k(\xi) \quad (3)$$

where $c_k^p(t)$ represents the time-varying coefficients. Assuming that the identity equation of F_{rk}^p is satisfied as:

$$F_{rk}^p = \int_A B_k(\xi) G_{pq}^r(x, \xi) dA(\xi) \quad (4)$$

Substituting the fault slip estimation models equations (3) and (4) into equation (1) yields the following observation model:

$$u_r(x,t) = \sum_{k=1}^{M} c_k^p(t) F_{rk}^p + L(x,t) + f(t) + e(x,t) \quad (5)$$

Let $m = 3(k-1) + p$ be defined, then the observation vector $\mathrm{d}_i(t)$ can be described as:

$$d_i(t) = \sum_{m=1}^{3M} c_m(t) F_m + L_i(t) + f_i(t) + e_i(t) \quad (6)$$

Interseismic deformation typically accumulates in a near-steady-state form [20]. The functional form of instantaneous deformation is difficult to predict and can only be described in a non-parametric manner as minor deviations from the steady-state deformation. Assuming that the slip is nearly stable, the NIF employs a stochastic model with a slip acceleration close to zero. The transient slip $\ddot{c}_m(t)$ is represented as a small increment:

$$\ddot{c}_m(t) = w_m(t) \quad (7)$$

where $w(t) \sim N(0, \alpha^2)$, $w(t)$ is white noise processes with a variance of α^2 in length^2/time^3. Perform a single integration on Equation (7):

$$\dot{c}(t) = \int_0^t dw(t')dt' = \alpha \dot{W}(t) + v \quad (8)$$

where dw represents white noise, $\dot{W}(t)$ denotes the transient slip rate resulting from the integration of Gaussian white noise, which is a given Brownian motion $B(t)$ random walk process [21-23], v is a

constant. The Brownian random motion model $B(t)$ is the integral of white noise:

$$B(t) = \int_0^t dw(t')dt' \tag{9}$$

where $w(t) \sim N(0, \tau^2)$, τ^2 has the unit of length^2/time.

Perform a second integration on Equation (8):

$$c(t) = \int_0^t B(t')dt' = W(t) + vt \tag{10}$$

where equation (9) satisfies $c(0) = 0$ at $t = 0$. The transient fault slip $W(t)$ is an integrated random walk process. The change of $W(t)$ from *t* to *t* + 1 is determined by α, and the long-term slip rate is given by v.

2.3 Filtering Process of the Algorithm

The NIF models the reference motion stochastic equations using a state space approach. The random system is represented using the state space method, where the state vector evolves linearly over time and is linearly related to the data. The state space approach does not require regular sampling of the data and can easily handle the issue of missing data at specific stations.

Let X_k denote the state vector at epoch $t_k (k = 0,1,2...)$, and the state-space model is represented by the nonlinear observation equation:

$$d_k = H_k X_k + e_k \tag{11}$$

where equation (11) relates the data H_k and state vector X_k, where *k* denotes the observation epoch, d_k is the data vector at the epoch *k*, $e_k \sim (0, R_k)$, and R_k is the covariance matrix of the observation noise.

The nonlinear state transition equation (12) describes the evolution of the state vector, predicting the state at epoch $k+1$ from the state at epoch *k*. The equation is given by:

$$X_{k+1} = T_{k+1} X_k + \delta_{k+1} \tag{12}$$

where $\delta_k \sim N(0, Q_{k+1})$, and Q_{k+1} is the covariance matrix of the process noise.

Random walk and integrated random walk can be represented using a state-space model. The random walk equation (9) is given by $X_k = B(t_k)$, and the state transition equation satisfies the form of a unit matrix:

$$T_k = I \tag{13}$$

where $Q_k = \tau^2 (t_k - t_{k-1})$ represents the covariance matrix. The state at time t_{k+1} is equal to the state at time t_k plus a random increment that is proportional to the time interval.

The state transition matrix T_k and the covariance matrix Q_k are defined as:

$$T_k = \begin{pmatrix} 1 & 0 & 0 \\ 0 & 1 & (t_k - t_{k-1}) \\ 0 & 0 & 1 \end{pmatrix} \tag{14}$$

$$Q_k = \begin{pmatrix} 0 & 0 & 0 \\ 0 & \alpha^2 \dfrac{(t_k - t_{k-1})^3}{3} & \alpha^2 \dfrac{(t_k - t_{k-1})^2}{2} \\ 0 & \alpha^2 \dfrac{(t_k - t_{k-1})^2}{2} & \alpha^2 (t_k - t_{k-1}) \end{pmatrix} \tag{15}$$

Equation (10) is modeled through the state vector:

$$X_k = \left[v, W(t_k), \dot{W}(t_k) \right]^{\mathrm{T}} \tag{16}$$

$$c(t_k) = \left[t_k, 1, 0 \right] X_k \tag{17}$$

The state vector for the integrated geodetic network is defined as:

$$X_k = [v_1, W_1(t_k), W_1(t_k), v_2, W_2(t_k), W_2(t_k), ..., v_M, W_M(t_k), W_M(t_k), B_1(t_k), B_2(t_k), ..., B_N(t_k)]^{\mathrm{T}} \tag{18}$$

where *M* denotes the number of basis functions, *N* represents the number of stations in the geodetic network. The length of the state vector is $3M + N$, with three components for each basis vector and one random walk component for each station.

The state transition matrix for the network inversion filtering has the following form:

$$T_k = \begin{pmatrix} T_k^W & 0 & 0 & 0 \\ 0 & \ddots & 0 & 0 \\ 0 & 0 & T_k^W & 0 \\ 0 & 0 & 0 & I_{N \times N} \end{pmatrix} \tag{19}$$

where comprises *M* submatrices T_k^W defined by Equation (14). The process covariance matrix is given as follows:

$$Q_k = \begin{pmatrix} Q_k^W & 0 & 0 & 0 \\ 0 & \ddots & 0 & 0 \\ 0 & 0 & Q_k^W & 0 \\ 0 & 0 & 0 & \tau^2 (t_k - t_{k-1}) I_{N \times N} \end{pmatrix} \tag{20}$$

where includes *M* submatrices Q_k^W defined by Equation (15). The observation matrix is given as

follows:

$$H_k = \left(F \begin{bmatrix} t_k & 1 & 0 & 0 & 0 & 0 & 0 \\ 0 & 0 & 0 & t_k & 1 & 0 & 0 \\ & & & & & & \ddots \end{bmatrix}, I_{N\times N} \right) \quad (21)$$

where submatrix F is defined by Equation (5) as an $N \times M$ matrix that maps the effect of each basis function onto the data. The $M \times 3M$ matrix within the brackets is pre-multiplied. The identity matrix $I_{N\times N}$ maps the local reference motion to each observation.

3. Result

3.1 Discrete subfaults

We employ GPS coordinate time series and the NIF method to invert the postseismic deformation in the Tokai region of Japan following the 2011 earthquake. It investigates the impact of the number of discrete subfaults in the regional fault model on the inversion process and the spatiotemporal evolution characteristics of the slip. According to the inversion results shown in Figure 2(a), the slip in the Tokai region primarily occurred between 34.8 °N and 35.8 °N and between 137.2 °E and 138.4 °E. The maximum cumulative slip reached 9.31 cm at the center, with a depth ranging from approximately 20 km to 60 km. Inverted propagation depth is slightly greater than the 50 km range reported in similar post-seismic slip studies by Silverii et al.[24]. This discrepancy is speculated to be due to the adoption of a different fault dislocation model, which can lead to variations in the inverted depth and slip[12]. Concurrently, multiple studies have indicated that observable slip can still occur at deeper fault sections (50-70 km), and that low-viscosity structures in the lower crust or asthenosphere can produce post-seismic relaxation effects at similar depths [25-27]. Therefore, the cumulative slip and depth range obtained from this study's inversion are deemed reasonable and physically plausible.

We varied the number of discrete subfaults by adjusting the grid spacing of the fault model. The grid spacings were set to 4.0 km, 5.0 km, 7.5 km, and 10.0 km, corresponding to approximately 5000, 3000, 1500, and 750 subfaults, respectively. The inversion times were approximately 22.89 h, 7.79 h, 1.39 h, and 0.61 h, while the maximum cumulative slip values were 8.84 cm, 9.31 cm, 10.77 cm, and 13.20 cm, respectively. The memory cost required was 842.0 G, 357.0 G, 82.2 G, and 29.3 G, respectively. The results indicate that within the same region, the smaller the grid spacing, the greater the number of subfaults, the longer the inversion time required, and the smaller the cumulative slip, which tends to stabilize at a certain value. It is inferred that this is because the NIF method establishes a connection between GPS stations and each discrete subfault through Green's functions, converting the surface displacement of the stations into slip on each subfault. Therefore, the greater the number of subfaults, the smaller the maximum cumulative slip of subfaults. The results indicate that the cumulative slip magnitude and depth obtained from fault models with grid sizes of 4 km and 5 km are generally consistent. Considering both computational efficiency and memory cost cost, a grid size of 5 km was ultimately selected as the standard for subsequent inversion analyses.

3.2 Proportionality parameters of the reference motion

The NIF assumes that the random reference motion follows a Brownian random walk process[13], which is a time-correlated low-frequency noise. Dmitrieva et al. developed a Network Noise Estimator (NNE) algorithm for estimating representative noise parameters in GPS coordinate time series[28]. This method is capable of accurately estimating random walk processes and provides better velocity uncertainty estimates compared to traditional single-station approaches. Dmitrieva et al. estimated the proportionality parameters of random walk using the NNE method, with the parameter range found to be approximately 0.1-1.5 mm/a$^{1/2}$. We refer to the settings of reference motion proportionality parameters by Langbein and Segall[13, 29] and tests the impact of different proportionality parameters τ on the time, memory cost, and maximum cumulative slip of NIF inversion of slow slip events.

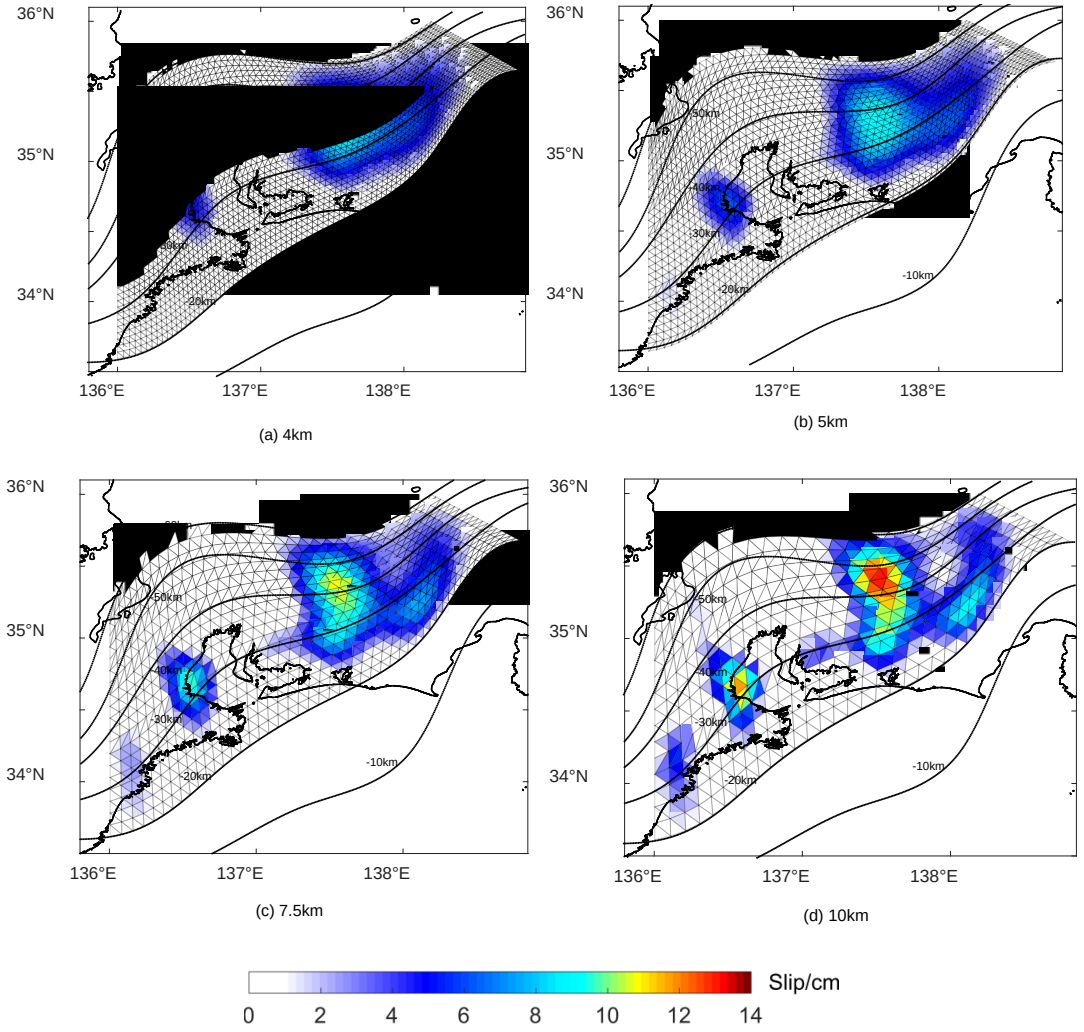

Figure 2. Fault slip distribution under different numbers of subfaults

As shown in Table 1 and Figure 3, variations in the random walk scale parameter have negligible effects on the inversion time and memory cost requirements for the NIF-based slow slip event inversions. However, the maximum cumulative slip exhibits a negative correlation with the random walk scale parameter. When the parameter approaches 0.1mm/$a^{1/2}$, the maximum cumulative slip tends to stabilize at a constant value.

Table 1. Influence of different reference motion scale parameters on time, memory cost and maximum cumulative slip of postseismic deformation by NIF

Proportionality parameters of the reference motion	Time/h	Memory cost/G	Maximum cumulative slip/cm
1.5mm/$a^{1/2}$	7.95	357	2.97
1mm/$a^{1/2}$	7.97	357	3.82
0.5mm/$a^{1/2}$	8.01	357	5.83
0.1mm/$a^{1/2}$	7.79	357	9.31
0.01mm/$a^{1/2}$	7.91	357	9.92
0.001mm/$a^{1/2}$	7.92	357	9.93

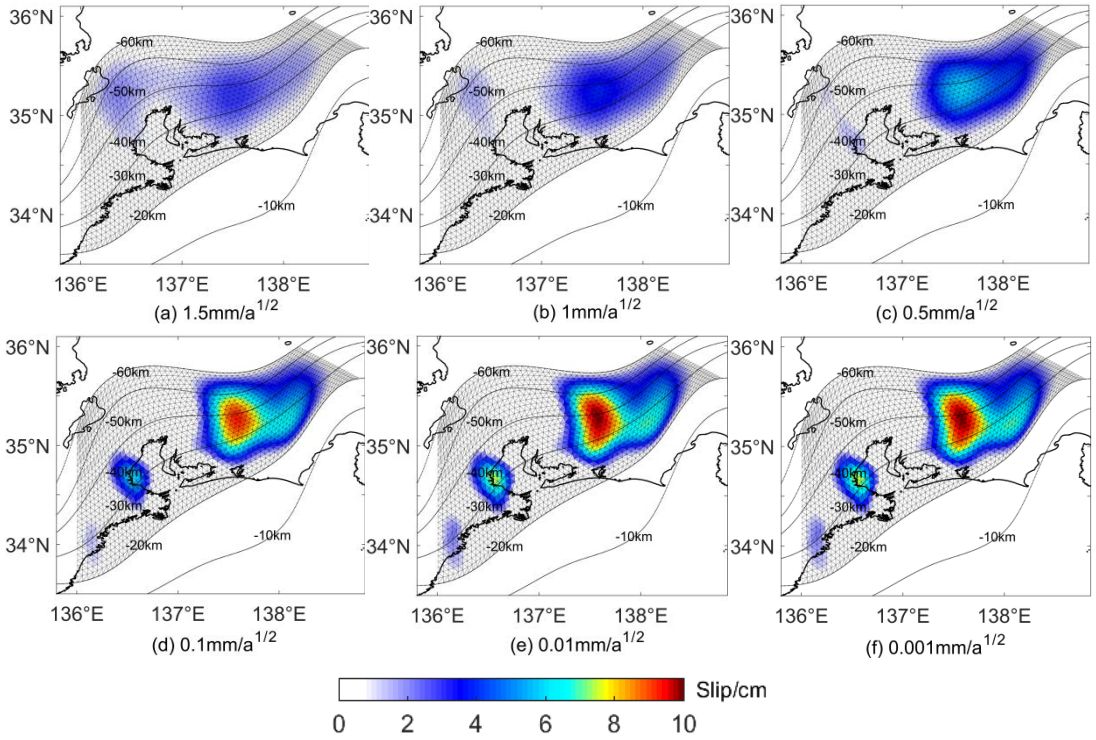

Figure 3. Fault slip distribution of different random reference motion scale parameters

3.3 Time scale

The time required, memory cost, maximum cumulative slip, and spatial distribution of cumulative slip for the NIF inversion of the postseismic deformation in the Tokai region from 2009 to 2021 are presented in Table 2 and Figures 4(a)-4(l). Using GPS coordinate time series with a sampling rate of 1 day in the Tokai region, the time and memory cost required for the NIF to invert the annual cumulative fault slip from 2009 to 2021 are consistent, with inversion times of approximately 7-9 hours and memory cost of about 330-360G. Following the occurrence of the 2011 Tohoku-Oki earthquake on March 11, the maximum annual fault slip in the Tokai region increased significantly to 9.31 cm. In the subsequent years, it gradually returned to the normal range of approximately 1-2 cm per year. Figure 4 shows the fault slip distribution before and after the postseismic deformation. The slip primarily occurred in the northeastern part of the Tokai region, at depths ranging from 20 to 60 km.

To clearly illustrate the temporal characteristics of slip, common mode error, and reference motion, we decompose the GPS slip time series of station J276 as an example, as shown in Figure 5. We selected the GPS coordinate time series of station J276 from 2015 to 2016 for decomposition, which is far from the time of the earthquake occurrence to avoid the influence of the earthquake on the estimation of common mode error. Based on the decomposition results, the variations in reference motion and common mode error are within 10 mm, which meets the error requirements.

This study is based on the GPS coordinate time series in the Tokai region from 2011 to 2021, using the NIF method to invert postseismic slip over a 2 year period. It compares whether the inversion results of slip from GPS coordinate time series over a 1 year timescale are additive to those over a 2 year timescale. The inversion results are presented in Table 3 and Figures 6a-6e. The time, memory cost, and maximum cumulative slip required for inverting the 1 year fault slip event are additive and essentially consistent with those required for inverting the 2 year slip event. Therefore, using single year GPS coordinate time series to invert and accumulate fault slip yields results that are generally consistent with those obtained from directly inverting multi year GPS coordinate time series.

Table 2. Inversion of every year postseismic deformation in the Tokai region

Year	Time/h	Memory cost/G	Maximum cumulative slip/cm
2009-2010	7.89	347	1.18
2010-2011	8.93	355	1.15
2011-2012	7.79	357	9.31
2012-2013	8.73	357	4.61
2013-2014	8.18	356	2.61
2014-2015	8.17	334	1.99
2015-2016	8.13	358	2.10
2016-2017	7.87	357	1.90
2017-2018	7.89	357	1.96
2018-2019	7.92	357	1.33
2019-2020	7.97	358	1.69
2020-2021	7.83	357	1.62

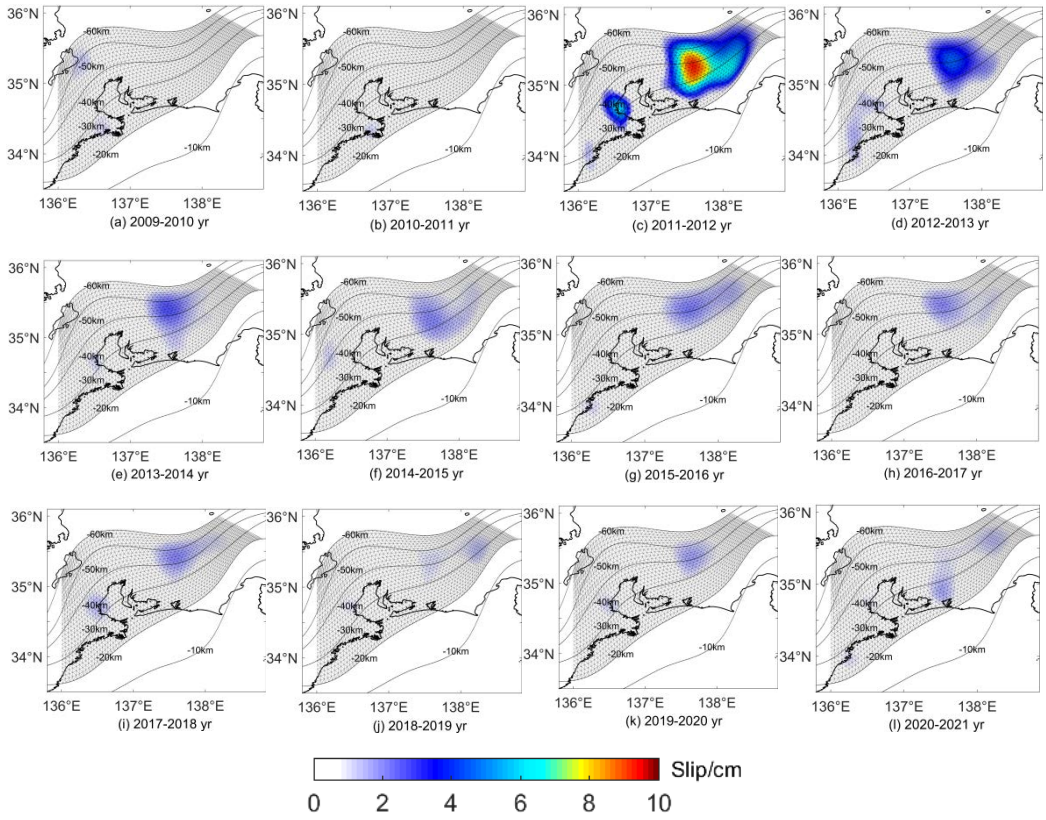

Figure 4. Distribution of every year fault slip in Tokai region

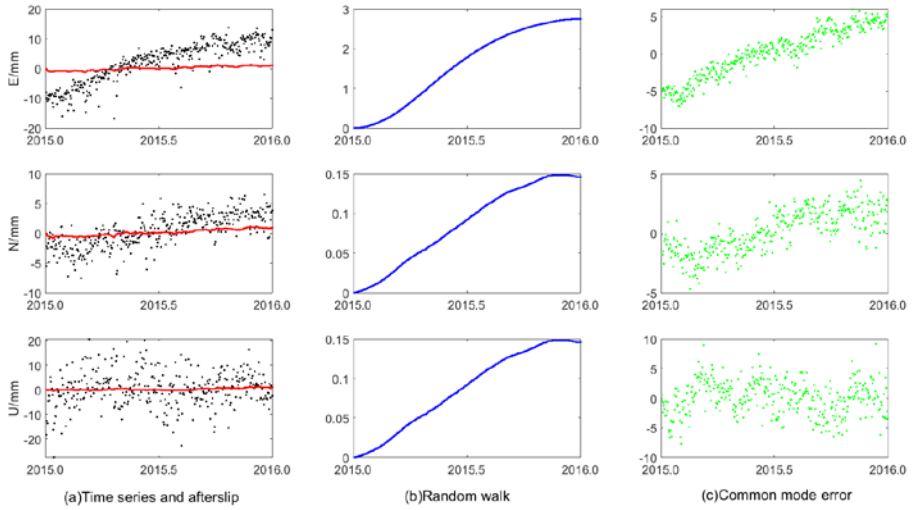

Figure 5. GPS afterslip displacement time series decomposition of J276

Table 3. Inversion of two years fault slip in the Tokai region

Year	Time/h	Memory cost/G	Maximum cumulative slip/cm
2011-2013	15.84	715	12.08
2013-2015	15.33	691	3.67
2015-2017	16.00	716	3.12
2017-2019	16.44	715	2.57
2019-2021	16.10	716	2.21

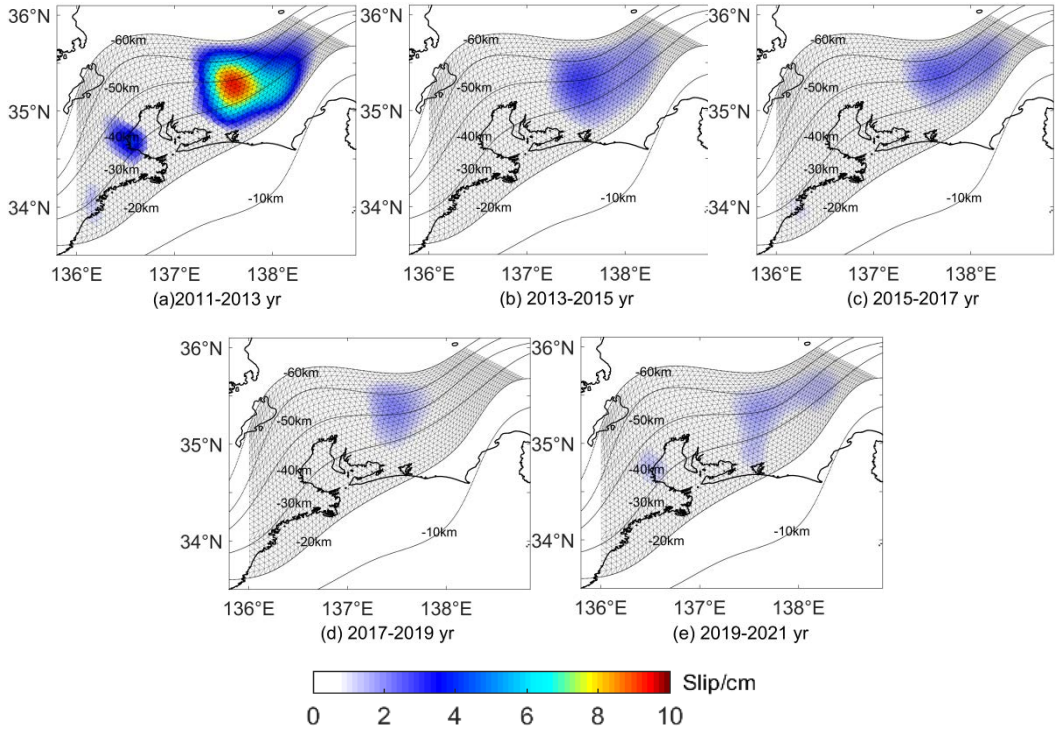

Figure 6. Distribution of two years fault slip in Tokai region

3.4 Temporal sampling rate

To assess the influence of varying temporal resolutions of GPS coordinate time series on the inversion results of postseismic deformation, the GPS data in the Tokai region were resampled to time intervals of 1, 3, 6, 12 and 24 days. Using the NIF method to invert the continuous 10 year fault slip in the Tokai region from 2011 to 2021 under different temporal resolutions, the required time, memory cost, and maximum cumulative slip are shown in Table 4. Table 4 show that the higher the temporal resolution of the GPS coordinate time series, the longer the inversion time required, the larger the memory cost needed, the more uniform the distribution of cumulative slip, and the smaller the difference in maximum cumulative slip. In the state model of the NIF , the state at time $t+1$ is equal to the state at time t plus a random increment that is proportional to the time interval. Therefore, the larger the time scale, the greater the random increment and consequently the larger the maximum cumulative slip. Figures 7(a)-7(e) show the spatial distribution of fault slip under different temporal resolutions. It can be seen that the higher the temporal resolution, the more uniform and smooth the spatial distribution of slip in the region. Conversely, the lower the temporal resolution, the larger the random increment, and the greater the inversion error that follows. In Figures 7(d) and 7(e), the temporal resolution of the GPS coordinate time series is too low, resulting in a discrete distribution of fault slip that no longer conforms to the spatial distribution characteristics of fault slip in slow slip events.

4. Conclusion

This study utilizes the NIF method to invert for postseismic deformation in the Tokai region, Japan, using GPS coordinate time series from 2009 to 2021. The research aims to investigate the efficiency of the NIF method and analyze the spatiotemporal evolution characteristics of regional fault slip. Taking the GPS coordinate time series in the Tokai region from 2009 to 2021 as an example, we inverted the spatiotemporal evolution characteristics of the fault slip in the Tokai region and tested the operational efficiency of the NIF method under different parameter conditions, such as the number of subfaults and the proportionality parameters of random reference motion. The conclusions are as follows:

(1) The NIF method was employed to invert the postseismic deformation following the 2011 earthquake in Tokai region of Japan, in order to obtain the spatiotemporal distribution of fault slip. The inversion results of the postseismic deformation event in the Tokai region indicate that the slip following the 2011 earthquake was primarily concentrated in the northeastern part of the Tokai region (34.8°N-35.8°N, 137.2°E-138.4°E), with a maximum cumulative slip of 9.31 cm at depths ranging from approximately 20 km to 60 km.

(2) Under different parameter conditions, the NIF inversion of postseismic deformation events exhibits distinct efficiency characteristics. Discrete subfaults were generated by setting the fault grid spacing, and postseismic deformation inversions were conducted with 750, 1500, 3000, and 5000 subfaults as preconditioning. The results show that as the number of subfaults increases, the required inversion time and memory cost increase, while the maximum cumulative slip approaches a stable value. Under the condition of local reference motion proportionality parameters ranging from 0.1 to 1.5 mm/$a^{1/2}$, there was no significant difference in inversion time and memory cost. As the proportionality parameter approached 0.1 mm/$a^{1/2}$, the maximum cumulative slip exhibited a negative correlation and tended to stabilize. The temporal scale of GPS coordinate time series has no significant impact on the inversion results using the NIF. Using GPS coordinate time series with different temporal resolutions and the NIF to invert postseismic deformation events, the inversion time and memory cost increase with the sampling rate of the GPS coordinate time series. The maximum cumulative slip tends to stabilize, and the regional slip distribution characteristics conform to the laws of slip propagation.

Table 4. Inversion of postseismic deformation from 2011 to 2021 at different time resolution GPS coordinate time series in Tokai region

Temporal sampling rate/d	Time/h	Memory cost/G	Maximum cumulative slip/cm
1	96.23	3470	13.8
3	28.81	1160	15.8
6	12.75	596	19.2
12	7.32	298	42.8
24	3.15	149	207

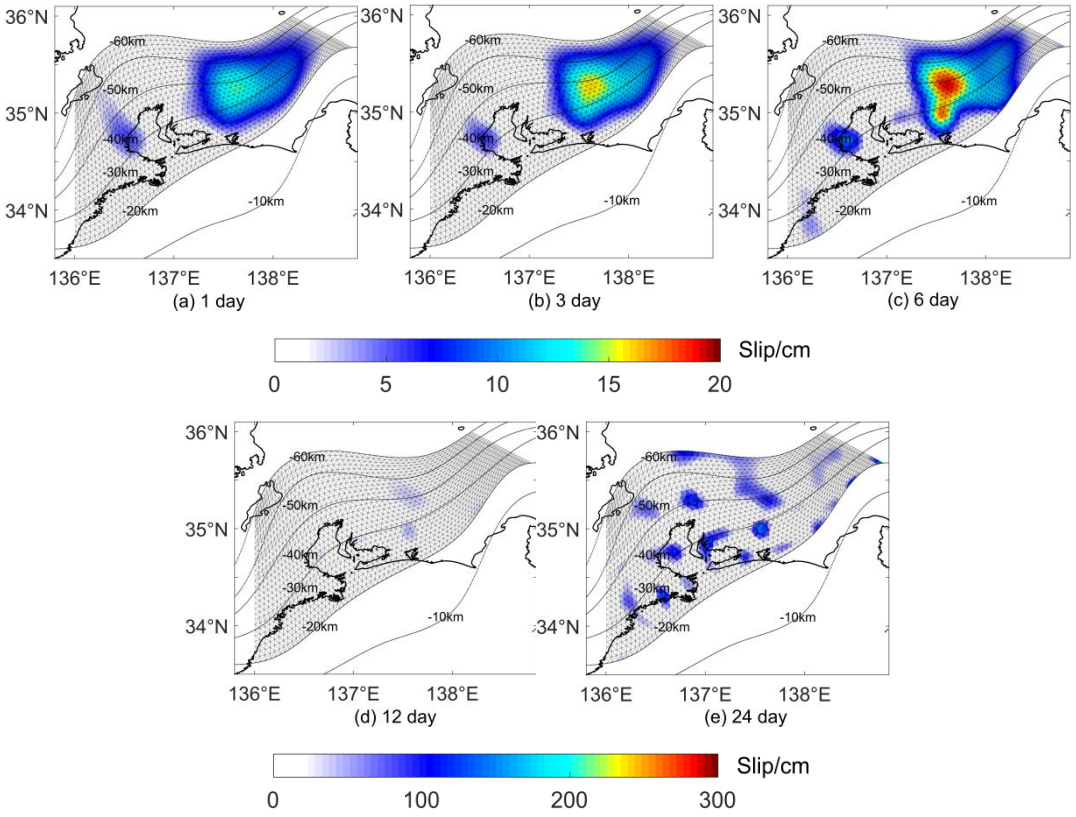

Figure 7. Distribution of fault slip from 2011 to 2021 at different time resolution GPS coordinate time series in Tokai region

References

[1] Nishimura, T., Hirasawa, T., Miyazaki, S., et al. Temporal change of interplate coupling in northeastern Japan during 1995-2002 estimated from continuous GPS observations. Geophysical Journal International, 2004, 157, 901-916. doi: 10.1111/j.1365-246X.2004.02159.x

[2] Perfettini, H., Avouac, J. P., Tavera, H., et al. Seismic and a Seismic Slip on the Central Peru Megathrust. Nature, 2010, 465(7294) , 78-81. doi: 10.1038/nature09062

[3] Jiang, W. P., Wang, K. H., Li, Z., et al. Prospect and Theory of GNSS Coordinate Time Series Analysis. Geomatics and Information Science of Wuhan University, 2018, 43(12), 2112-2123. doi: 10.13203/j.whugis20180333

[4] Wang, R., Xia, Y., Grosser, H., et al. The 2003 Bam(SE Iran) Earthquake:Precise Source Parameters from Satellite Radar Interferometry. Geophysical Journal International, 2004, 159(3), 917-922. doi: 10.1111/j.1365-246X.2004.02476.x

[5] Sun, H., Ji, L. Y., Zhu, L. Y., et al. Coseismic Deformation and Postseismic Deformation

Mechanism Yutian M_s7.3 Earthquake. Journal of Geodesy and Geodynamics, 2016, 36(12), 1052-1055+1068.

[6] Wang, R., Parolai, S., Ge, M., et al. The 2011 Mw9.0 Tohoku Earthquake: Comparison of GPS and Strong-Motion Data. Bulletin of the Seismological Society of America, 2013, 103(2B), 1336-1347.

[7] Hong, S. Y., Dong, Y. F., Meng, G. J., et al. Postseismic deformation extraction and afterslip inversion of the October 2008 Damxung M_w6.3 earthquake. Chinese Journal of Geophysics, 2018, 61(12), 4827-4837. doi: 10.6038/cjg2018L0437

[8] Li, S. P., Chen, G., He, P., et al. Inversion for Coseismic Slip Distribution and Afterslip of the 2015 Nepal Mw 7.9 Earthquake Using Angular Dislocations. Geomatics and Information Science of Wuhan University, 2019, 44(12), 1787-1796. doi: 10.13203/j.whugis20180128

[9] Yang, Z. R., Yuan, L. G., Jiang, Z. S., et al. Temporal-Spatial Distribution of Post-Seismic Afterslip Associated with the 2015 Mw7.9 Nepal Earthquake. Journal of Geodesy and Geodynamics, 2018, 38(9), 891-896.

[10] Li, M., Yan, L., Jiang, Z. S., Xiao G R. Insights into spatio-temporal slow slip events offshore the Boso Peninsula in central Japan during 2011-2019 using GPS data. Geodesy and Geodynamics, 2022, 13(6), 554-563.

[11]Yamagiwa, S., Miyazaki, S., et al. Afterslip and viscoelastic relaxation following the 2011 Tohoku-oki earthquake (Mw9.0) inferred from inland GPS and seafloor GPS/Acoustic data. Geophysical Research Letters, 2015, 42(1), 66-73. doi: 10.1002/2014GL061735

[12]Liu, T., Fu, G. Y., Zhou, X., Su, X. N. Mechanism of post-seismic deformations following the 2011 Tohoku-Oki MW9.0 earthquake and general structure of lithosphere around the source. Acta Geophysica Sinica, 2017, 60(9), 3406-3417. doi: 10.6038/cjg20170911

[13] Segall, P., Matthews, M. Time dependent inversion of geodetic data. Journal of Geophysical Research, 1997, 102(B10), 22391. doi: 10.1029/97JB01795

[14] Mccaffrey, R. Time-dependent inversion of three-component continuous GPS for steady and transient sources in northern Cascadia. Geophysical Research Letters, 2009, 36(7), L07304. doi: 10.1029/2008GL036784

[15] Yoshioka, S., Matsuoka, Y., Ide, S. Spatiotemporal slip distributions of three long-term slow slip events beneath the Bungo Channel, southwest Japan, inferred from inversion analyses of GPS data. Geophysical Journal International, 2015, 201(3), 1437-1455. doi: 10.1093/gji/ggv022

[16] Radiguet, M., Cotton, F., Vergnolle, M., et al. Spatial and temporal evolution of a long term slow slip event: The 2006 Guerrero Slow Slip Event. Geophysical Journal International, 2011, 184(2), 816-828. doi: 10.1111/j.1365-246X.2010.04866.x

[17]Suenaga, N., Yoshioka, S., Matsumoto, T. Relationships among temperature,dehydration of the subducting Philippine Sea plate,and the occurrence of a megathrust earthquake, low-frequency earthquakes,and a slow slip event in the Tokai district,central Japan. Physics of the Earth and Planetary Interiors, 2016, 260, 44-52. doi: 10.1016/j.pepi.2016.09.004

[18]Ozawa, S., Nishimura, T., et al. Coseismic and postseismic slip of the 2011 magnitude-9 Tohoku-Oki earthquake. Nature, 2011, 475(7356), 373-376. doi: 10.1038/nature10227

[19]Simons, M., Minson, S. E., et al. The 2011 Magnitude 9.0 Tohoku-Oki Earthquake: Mosaicking the Megathrust from Seconds to Centuries. Science, 2011, 332(6036), 1421-1425. doi: 10.1126/science.1206731

[20] Savage, J. C., Lisowski, M. Interseismic deformation along the San Andreas Fault in southern California. Journal of Geophysical Research Solid Earth, 1995, 100(B7), 12703-12717. doi: 10.1029/95JB01153

[21] Wyatt, F. K. Displacement of surface monuments: Horizontal motion. Journal of Geophysical Research, 1982, 87(B2), 979. doi:

10.1029/JB087iB02p00979

[22] Wyatt, F. K. Displacement of surface monuments: Vertical motion. Journal of Geophysical Research Solid Earth, 1989, 94(B2). doi: 10.1029/JB094iB02p01655

[23]Langbein, J., Johnson, H. Correlated errors in geodetic time series: Implications for time-dependent deformation. Journal of Geophysical Research, 1997, 102(B1), 591. doi: 10.1029/96JB02945

[24]Silverii, F., Cheloni, et al. Post-seismic slip of the 2011 Tohoku-Oki earthquake from GPS observations: implications for depth-dependent properties of subduction megathrusts. Geophysical Journal International, 2014, 198(1), 580-596. doi: 10.1093/gji/ggu149

[25]Sun, T. H. Z., Wang, K. L., et al. Prevalence of viscoelastic relaxation after the 2011 Tohoku-oki earthquake. Nature, 2014, 514(7520), 84-87. doi: 10.1038/nature13778

[26]Diao, F. Q., Xiong, X., et al. Overlapping post-seismic deformation processes: afterslip and viscoelastic relaxation following the 2011 M-w 9.0 Tohoku (Japan) earthquake. Geophysical Journal International, 2014, 196(1), 218-229. doi: 10.1093/gji/ggt376

[27]Iinuma, T., Hino, R., et al. Seafloor observations indicate spatial separation of coseismic and postseismic slips in the 2011 Tohoku earthquake. Nature Communications, 2016, 7(1), 13506. doi: 10.1038/ncomms13506

[28] Dmitrieva, K., Segall, P., DeMets, C. Network-based estimation of time-dependent noise in GPS position time series. Journal of Geodetic Science, 2015, 89, 591-606. doi: 10.1007/s00190-015-0801-9

[29]Langbein, J., Johnson, H. Correlated errors in geodetic time series: Implications for time-dependent deformation. Journal of Geophysical Research, 1997, 102(B1), 591. doi:10.1029/96JB02945

Authors

Zhengdong Luo is currently a Ph.D. candidate at the School of Surveying and Geoinformation Engineering, East China University of Technology. His research interests include GNSS deformation monitoring and inversion.

Tieding Lu is a Professor at the School of Surveying and Geoinformation Engineering, East China University of Technology. His main research interests include GNSS data processing and navigation.

Qianru Chen is currently a Ph.D. candidate at the School of Surveying and Geoinformation Engineering, East China University of Technology. His research interests include GNSS data processing and navigation.

Xiwen Sun is currently a Ph.D. candidate at the School of Surveying and Geoinformation Engineering, East China University of Technology. Her main research interests include Space Geodesy and Remote sensing of Environment.

Weijian Hu is currently a Ph.D. candidate at the School of Surveying and Geoinformation Engineering, East China University of Technology. His research interests include GNSS data processing.